Development patterns of the dynamic elastic modulus of saturated coral sand under different drainage conditions

Ruirong Zhou[1,2], Zhilei Huo[3], Qifei Liu[2]*, Qingquan Yu[1,4] and Qi Wu[2]

[1]School of Civil Engineering, Sanjiang University, Nanjing, China, [2]Institute of Geotechnical Engineering, Nanjing Tech University, Nanjing, China, [3]China Nuclear Power Engineering co., Ltd., Beijing, China, [4]Jiangsu Engineering Research Center for Low Carbon Materials and Green Structures, Nanjing, China

Long-term cyclic loading can have a significant effect on the modulus of sand, and the influence on saturated coral sand has yet to be established. In this paper, the significant influence of non-plastic fines content (FC) and relative density (D_r) on dynamic elastic modulus (E) of saturated coral sand has been evaluated by a series of cyclic triaxial drainage tests. The results show that the dynamic elastic modulus increases rapidly at the beginning of loading; then the growth slows down and finally stabilizes. In general, the development of E is influenced collectively by FC, D_r and cyclic stress ratio (CSR). The initial dynamic elastic modulus E_{d-1} and steady-state dynamic elastic modulus E_{d-s} increase with the increase of D_r, and decrease as FC increases. The linear fitting equations are given by introducing the equivalent skeleton void ratio e_{sk}*. Furthermore, the relative dynamic elastic modulus E_r is defined as the ratio of E_{d-N} to E_{d-s}, and the prediction equation for E_r was developed to provide a basis for the engineering mechanical parameters of coral sands under long-term loads.

KEYWORDS

saturated coral sand, dynamic elastic modulus, relative density, equivalent skeleton void ratio, cyclic triaxial drainage test

1 Introduction

The carbonate sand formed by marine biological deposition, whose $CaCO_3$ content is >90%, is referred to as coral sand. Coral sand is abundant in nature (e.g. in the Persian Gulf and the South China Sea) and is often used as the primary geotechnical material for constructing infrastructures such as coral islands and reefs or harbors (Ding et al., 2021). Coral islands and reefs or harbors are located in marine environments that are susceptible to dynamic loads from long-term waves, storm surges, tsunamis, and earthquakes. Differential subsidence or permanent deformation caused by these marine dynamic

loads can have a remarkable impact on the foundations of coral sand (Wen et al., 2021). During analysis of soil dynamics problems, the dynamic elastic modulus of the soil is considered a key parameter for studying the soil's ability to resist deformation (Seed and Idriss, 1970; Rollins et al., 1998, 2020; Chen et al., 2024; Ma et al., 2024a). This modulus effectively reveals the complex nonlinear relationship between dynamic stress and strain in soils, thereby providing an important theoretical basis for investigating the dynamic properties of soils. The dynamic elastic modulus of a sandy soil is an important parameter when describing its deformation features under dynamic loading. In the fields of earthquake, foundation, and geotechnical engineering, the dynamic elastic modulus is one of the key indicators for assessing the response of a sandy soil under seismic or other dynamic loads.

There are many researches on the dynamic deformation characteristics of soils in different regions, but most of the researches devoted to clay and granular soils (Iwasaki et al., 1978; Kallioglou et al., 2008; Vucetic and Mortezaie, 2015; Kantesaria and Sachan, 2021; Nong. and Park, 2021), studies on the dynamic elastic modulus of coral sand are rather limited. Long et al. (2022) investigated the impact of coral sand grain breakage on its dynamic properties. The result of resonant column tests indicated that the maximum dynamic shear modulus (G_{max}) of the coral sand first increased and then decreased with the increase in the degree of coral sand grain breakage. Furthermore, Wu et al. (2022) conducted a series of resonant column tests on coral sand with different fines content (FC) and found that the shear modulus ratio G/G_{max} - shear strain γ curves show FC-dependent development and are characterized by nonlinear enhancement with increasing FC. Catano and Pando (2012) investigated the CaboRojo coral sand and found the shear modulus G value of coral sand was smaller than that of quartz sand. Alternatively, Jafarian and Javdanian (2020) investigated the Bushehr coral sand using the resonant column technique and found that the relative density had a minor impact on the dynamic shear modulus ratio. While, the decay of G/G_{max} gradually slows down as the effective confining pressure increases. Liang et al. (2023) studied the small-strain shear modulus G_0 of coral sands from Nansha and Xisha Islands. A G_0 prediction model for different types and gradations of sandy soils is proposed by introducing the concept of critical porosity ratio. Wichtmann et al. (2015) focused on the impacts of FC on G_{max} of quartz sands. At the same porosity ratio e, when $FC< 10\%$, G_{max} decreases substantially with increasing FC; when $FC = 10\%–20\%$, G_{max} increases with increasing FC; however, when FC is >20%, G_{max} does not change significantly with FC. These findings provide an important basis for a deeper understanding of the impacts of FC on the mechanical properties of quartz sands.

Previous studies have investigated the development of G of sands within small strain conditions using resonant column tests. In this study, the drained cyclic triaxial tests have been conducted to study the influence of FC and relative density (D_r) on the initial dynamic elastic modulus ($E_{d\text{-}1}$) and steady-state dynamic elastic modulus ($E_{d\text{-}s}$). Based on the experimental results, a prediction equation for the relative elasticity modulus ratio (E_r) is given, so as to provide a basis for the engineering mechanical parameters of coral sands with non-plastic fines under long-term loads.

2 Test materials and methods

2.1 Test materials

The coral sand from a reef in the Nansha Islands was used for testing, which is a unique marine soil formed from the remains of marine organisms through physical, chemical, and biological processes. The coral sand grains are mainly composed of aragonite, high-magnesium calcite, and 90% $CaCO_3$. It is a calcareous sand with a specific gravity of 2.84. Coral sands are widely distributed in tropical and subtropical waters, and extensively found across China's Nansha Islands, serving as the primary geotechnical media with yellowish–white grains in the Nansha Islands area. The coral sand used in this study was found in the complex marine environment of the Nansha Islands, which results in several distinctive properties of coral sand grains: they are angular, prone to cementation and breakage, and have rough surfaces and internal pores (Karatza et al., 2017; Deng and Haigh, 2022).

The coral sand was first dried in a constant temperature oven at 103°C. Then, to separate the fine grains of the coral sand from the sand grains, the coral sand was sifted using a standard sieve with a mesh size of 0.075 mm. This process allowed the separation of two types of coral sand grains based on the 0.075-mm threshold (Zhao et al., 2022). Coral sand grains<0.075 mm were considered as fine grains, while those above this size were considered sand grains. Fine particles have no discernible liquid or plastic limit and are classified as non-plastic particles (ASTM International, 2000). Fine and sand grains of different masses were uniformly mixed to obtain coral sands with different FC. The gradation curves of pure sand, pure fine, and coral sand grains with different FCs are shown in Figure 1. Figure 1 lists the basic physical indicators of the coral sand. The maximum and minimum porosity ratios were measured according to ASTM specifications. To avoid changes in grain size distribution due to breakage during measurement, the minimum porosity ratio was measured using the vibration metho (ASTM D4253, 2016a; and ASTM D4254, 2016b).

2.2 Test apparatus and sample preparation

A GDS cyclic triaxial apparatus was used for performing stress-controlled drainage cyclic loading tests. This apparatus applies a maximum axial stress of ±5 kN with an accuracy of up to 0.001 kN. The confining pressure chamber can withstand a maximum pressure of 2 MPa. The axial displacement range is 100 mm with a displacement accuracy of 0.07% F.S (full scale). To ensure the uniformity of coral sand with fine grains, samples were prepared using the dry sampling method with a diameter of $D = 50$ mm and a height of $H = 100$ mm. According to gradations shown in Figure 1, the sand required for each specimen was weighed and evenly divided into five layers for filling into film-bearing cylinders. During the filling process, the layer height was strictly controlled, and the surface of each layer was brushed to ensure uniformity. Upon completion of sample preparation, CO_2 was introduced to displace air, followed by presaturation using air-free water. Then,
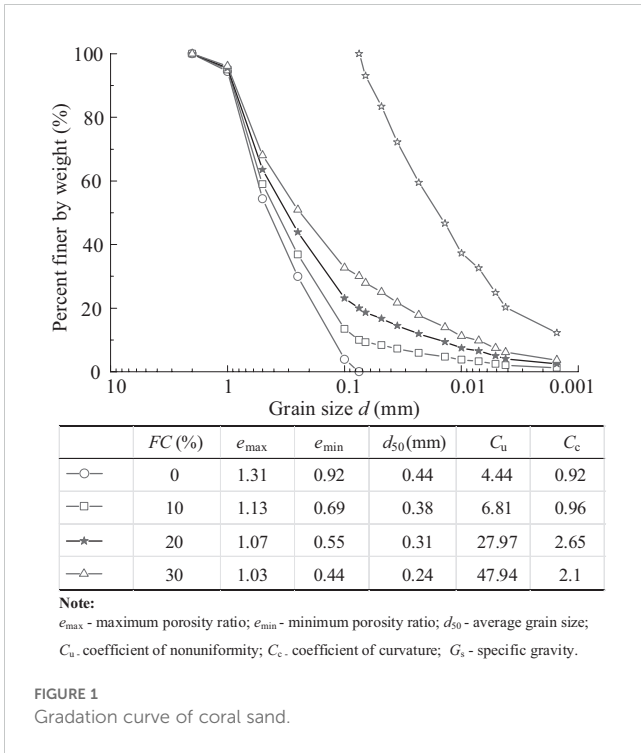
FIGURE 1
Gradation curve of coral sand.

$$E_d = \frac{\sigma_d}{\varepsilon_d} \qquad (2a)$$

where, σ_d and ε_d are axial dynamic stress and strain, respectively.

Under cyclic loading, the contact force between saturated coral sand grains gradually increases with increasing soil density, thereby increasing the dynamic elastic modulus E_d. When the dynamic elastic modulus stabilizes, the contact force between grains remains the same and E_d reaches a steady state. The average dynamic elastic modulus of saturated coral sand at the N-th cycle id denoted as $E_{d\text{-}N}$. Figure 2 illustrates the calculation of $E_{d\text{-}N}$ using Equation 2b.

$$E_{d-N} = \frac{\sigma_{d,max} - \sigma_{d,min}}{\varepsilon_{d,1} - \varepsilon_{d,2}} \qquad (2b)$$

Where $\sigma_{d,max}$ and $\sigma_{d,min}$ are the maximum and minimum cyclic deviatoric stresses at the Nth cycle, and $\varepsilon_{d,1}$ and $\varepsilon_{d,2}$ are the axial strains corresponding to $\sigma_{d,max}$ and $\sigma_{d,min}$, respectively. Figure 3 shows the curve of dynamic elastic modulus of the saturated coral sand $E_{d\text{-}N}$ versus N. As shown in this figure, $E_{d\text{-}N}$ accumulates continuously with increasing N. It increases rapidly at the beginning of loading; then, its growth rate slows down until it stabilizes. During loading, the dynamic elastic modulus of the saturated coral sand increases with the increase in the relative density D_r; the growth rate of $E_{d\text{-}N}$ decreases with increasing D_r and increases with increasing FC and CSR.

3.1 Analysis of the initial dynamic elastic modulus

In this study, the dynamic elastic modulus $E_{d\text{-}1}$ at the first cycle $N = 1$ is defined as the initial dynamic elastic modulus. Figure 4 shows the relationship curve between the initial dynamic elastic modulus $E_{d\text{-}1}$ and FC. With FC ranging from 0 to 30%, the initial dynamic elastic modulus decreases with increasing FC and CSR and increases with increasing D_r. Thus, the magnitude of the initial dynamic elastic modulus is affected by FC, D_r, and CSR. This is because for D_r, the number of sand grains that make up the soil skeleton decreases gradually with the increase of FC and some of them are replaced by fine grains, thus decreasing the stiffness of the

the samples were saturated using the graded back pressure saturation method. When the measured pore pressure coefficient B was ≥0.97, the samples were considered fully saturated. After saturation, an initial effective confining pressure $\sigma_m{}'$ = 100 kPa was uniformly applied for consolidation.

2.3 Test scheme

To investigate the development patterns of volumetric strain of coral sands with different D_r, FC, and cyclic stress ratio (CSR) values under cyclic drainage loading conditions, coral sands with FC = 0%, 10%, 20%, and 30% were used to prepare samples with D_r = 30%, 50%, and 70%, respectively, followed by uniform consolidation at σ'_m = 100 kPa. After consolidation, drainage cyclic loading tests with CSR = 0.20, 0.25, and 0.30, were conducted. The detailed test scheme is shown in Table 1, with *CSR*:

$$CSR = \frac{\sigma_d}{2\sigma'_m} \qquad (1)$$

where σ_d is the cyclic deviatoric stress. The test was performed using sine waves with a loading frequency of 0.1 Hz.

3 Test results and analysis

There is relatively limited documentation on how to use a dynamic triaxial apparatus to test the coral sand from the South China Sea under drainage cyclic loading conditions to obtain its dynamic elastic modulus. Hence, the analysis of the dynamic modulus of the soil is crucial, which is defined as:
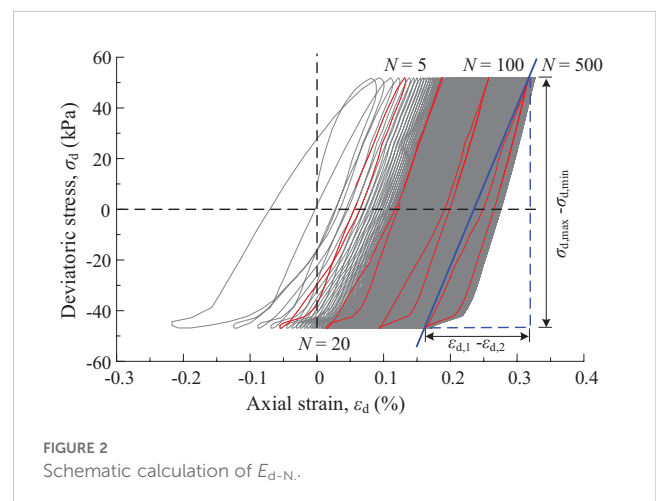

FIGURE 2
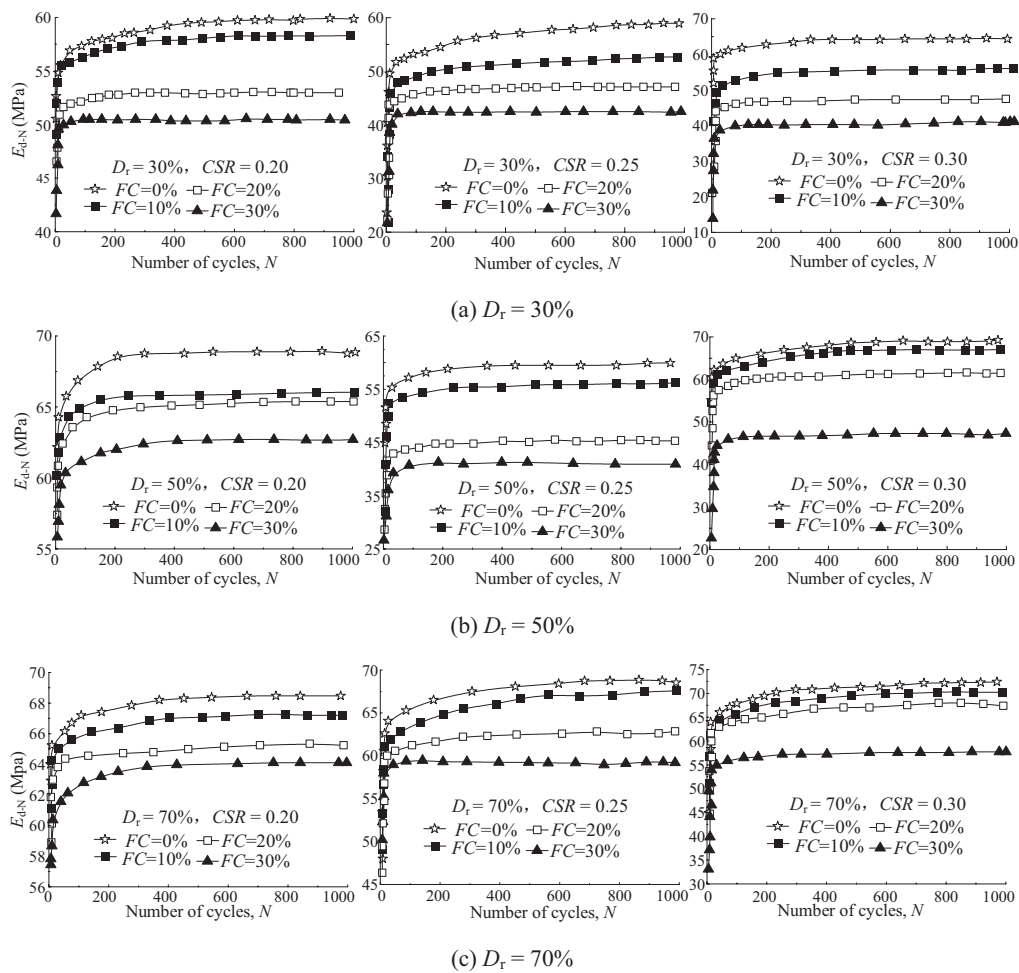Schematic calculation of $E_{d\text{-}N}$.

FIGURE 3
Development of dynamic elastic modulus E_{d-N} of saturated coral sand with N. **(A)** D_r = 30%, **(B)** D_r = 50%, **(C)** D_r = 70%.

sample in the initial state and E_{d-1}. With the increase of D_r, the degree of compaction of the sample increases and the contact between grains is closer, thus increasing the stiffness of the sample and E_{d-1}. The above analysis indicates that the impacts of the composition of grains on E_{d-1} cannot be reasonably characterized by FC or D_r alone. Thevanayagam (2000) proposed the equivalent skeleton void ratio $e_{sk}{}^*$ considering influence of fines on the contact of sand particles and the interparticle contact force

chain. The formula is as follows:

$$e_{sk}^* = \frac{e + (1 - b) \times FC}{1 - (1 - b) \times FC} \qquad (3)$$

where e is void ratio, b is the proportion of fines involved in the force chain between soil particles on the premise that FC is smaller than the threshold fines content FC_{th} (FC_{th} = 30% for the coral sand in this study). The parameter b is calculated using the semi-
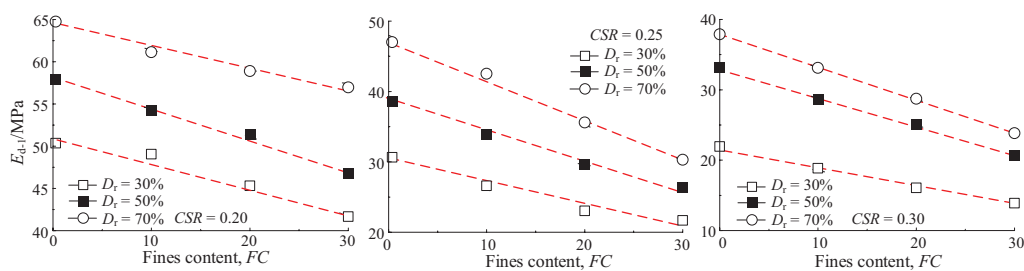

FIGURE 4
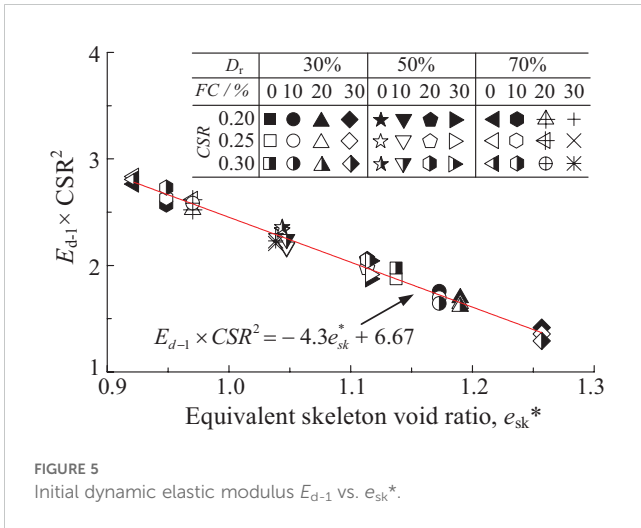Curve of initial dynamic elastic modulus E_{d-1} versus fines content FC.

FIGURE 5
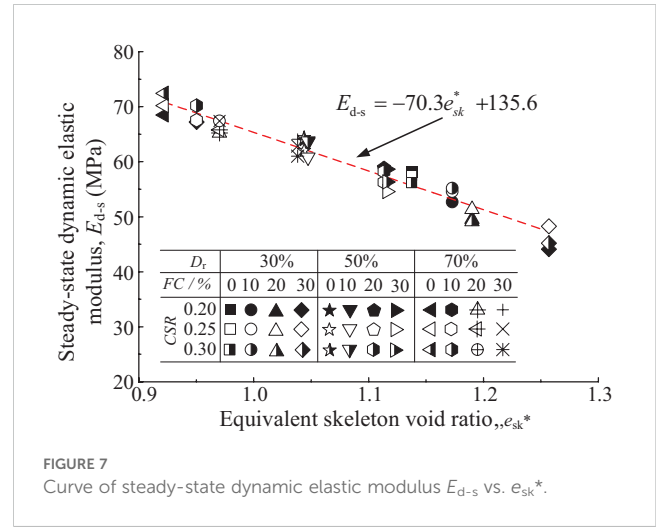Initial dynamic elastic modulus E_{d-1} vs. e_{sk}^*.

FIGURE 7
Curve of steady-state dynamic elastic modulus E_{d-s} vs. e_{sk}^*.

empirical formula proposed by Rahman et al. (2008) and Mohammadi and Qadimi (2015), and its validity has been verified by Chen et al. (2020).

Therefore, the equivalent skeleton void ratio e_{sk}^* is used to characterize E_{d-1}. It can be found that E_{d-1} decreases with the increase of e_{sk}^*, indicating a clear relationship between E_{d-1} and e_{sk}^*; e_{sk}^* is an appropriate physical indicator for characterizing E_{d-1}. As shown in Figure 5, a clear linear relationship between the CSR-corrected initial dynamic elastic modulus and equivalent porosity ratio of the skeleton is established:

$$E_{d-1} \times CSR^2 = -4.3e_{sk}^* + 6.67 \tag{4}$$

3.2 Analysis of the steady-state dynamic elastic modulus

When the volumetric strain ($\Delta\varepsilon_v$) development plateaus during drained cyclic loading ($\Delta\varepsilon_v/\Delta N < 0.01$), the specimen is considered to have reached steady state. The E_{d-N} in this state is defined as the steady-state dynamic elastic modulus E_{d-s}. The variation in the steady-state dynamic elastic modulus E_{d-s} is affected by D_r and FC,

as shown in Figure 6. According to the experimental results, E_{d-s} decreases with increasing D_r, and increases linearly with decreasing FC. In addition, the experimental results show that E_{d-s} increases slightly with increasing CSR. This is consistent with the finding of Ma et al. (2024b) that elastic modulus increases slightly with increasing strain rate.

When E_{d-N} reaches E_{d-s} at a given D_r, it indicates that the sample has reached the maximum degree of compaction under the applied stress. When FC< FC_{th}, fine grains fill in between the coarse particle skeleton or wrapped around the surface of the coarse sand, and their lubricating effect reduces the stiffness of the soil. This observation is consistent with the findings Huang et al. (2023) obtained using the three-dimensional discrete element method. The greater the FC, the more the fine grains in the soil skeleton, thus remarkably reducing the stiffness. An increase in the initial D_r would increase the degree of compaction of the consolidated sample, which strengthens the contact interaction between soil grains and manifests itself as an increase in the dynamic elastic modulus.

The equivalent skeleton void ratio e_{sk}^* is introduced to characterize the combined impact D_r and FC. As shown in Figure 7, a clear linear correlation exists between D_r and FC, which allows us to conclude that
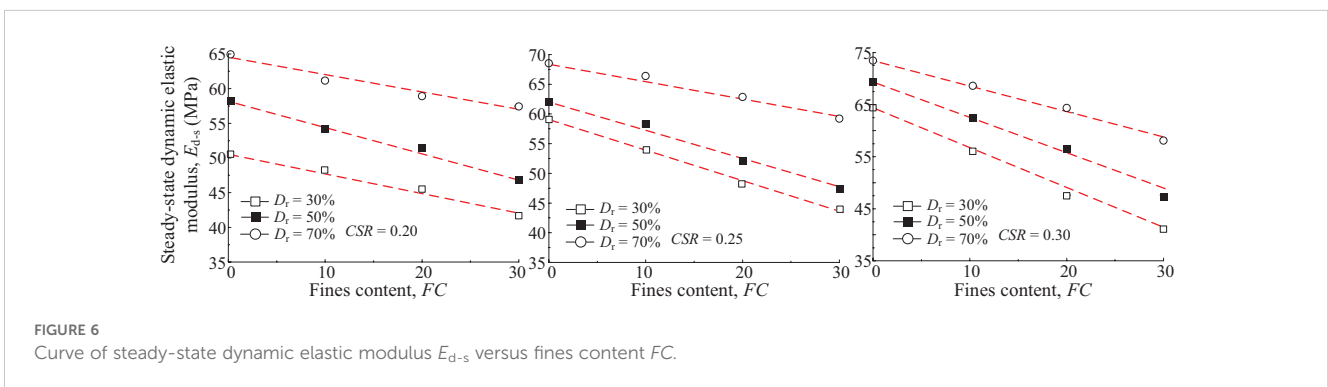

FIGURE 6
Curve of steady-state dynamic elastic modulus E_{d-s} versus fines content FC.

$$E_{d-s} = -70.3e_{sk}^{*} + 135.6 \qquad (5)$$

3.3 Prediction modeling for the relative dynamic elastic modulus

The ratio of E_{d-N} to E_{d-s} is defined as the relative dynamic elastic modulus E_r (Equation 6). E_r represents the stability development of the coral sand under cyclic drainage loading and is of guidance for the foundation design under long-term loading.

$$E_r = \frac{E_{d-N}}{E_{d-s}} \qquad (6)$$

Figure 8 shows the development curve of the relative dynamic elastic modulus E_r with the number of cycles N. It can be seen that the degrees of discreteness of E_r–N curves at different FCs and the same D_r are extremely small, indicating that FC has almost no impact on the development of E_r with N.E_r eliminates the impact of various FC, and during cyclic loading, E_r develops with N in the form of an approximate inverse tangent function.

$$E_r = A \arctan[B \times (N + 1)] \qquad (7)$$

Equation 7 was used to analyze the development of E_r, namely, parameters A and B. A mathematical analysis indicated that parameter A is related to the final value of the relative dynamic elastic modulus E_r, while parameter B is a variable related to the growth rate of E_r. According to the A–B relationship shown in Figure 9, parameter A is related to the soil, and remains constant at 0.63 for the saturated coral sand used in this study, unaffected by FC, CSR, or D_r. The growth rate of the E_r is affected by the combined impact of FC, CSR, and D_r. When the impact of FC is eliminated, changes in D_r will substantially affect the fitting parameter B. The value of B shows a linear increase with increasing D_r. This is because an increase in the D_r would increase the degree of compaction of the loaded sample, which strengthens the contact interaction between soil grains and manifests itself as an increase in the dynamic elastic modulus.

Parameter B is corrected by CSR, and in this study, the density correction parameter D_r^{CSR} is used in place of the relative density D_r. As shown in Figure 10, there is a clear linear relationship between the two.

$$B \times CSR = 0.036 + 0.16D_r^{CSR} \qquad (8)$$

Thus, a prediction model for the dynamic elastic modulus of saturated coral sands can be developed as follows:
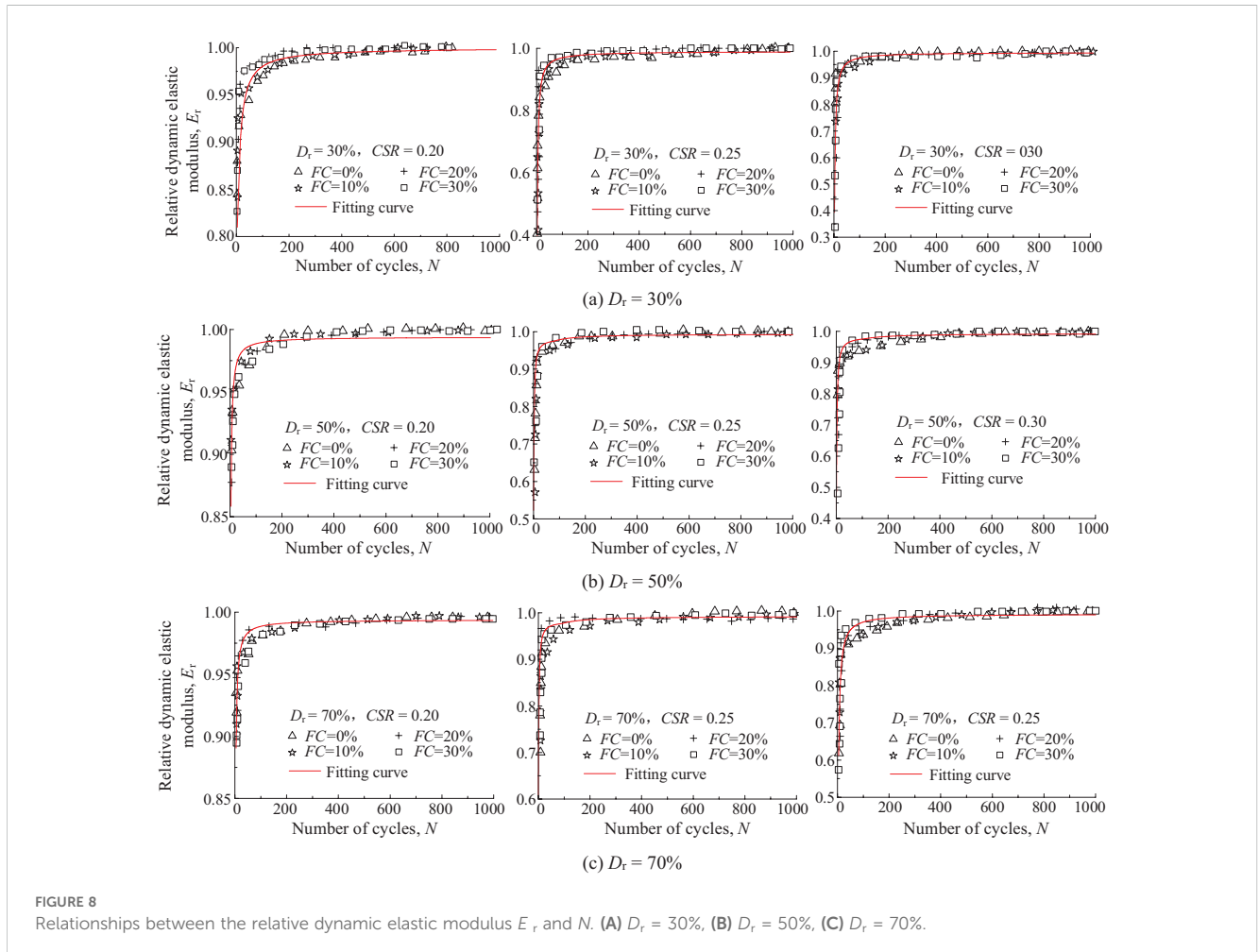

FIGURE 8
Relationships between the relative dynamic elastic modulus E_r and N. **(A)** D_r = 30%, **(B)** D_r = 50%, **(C)** D_r = 70%.
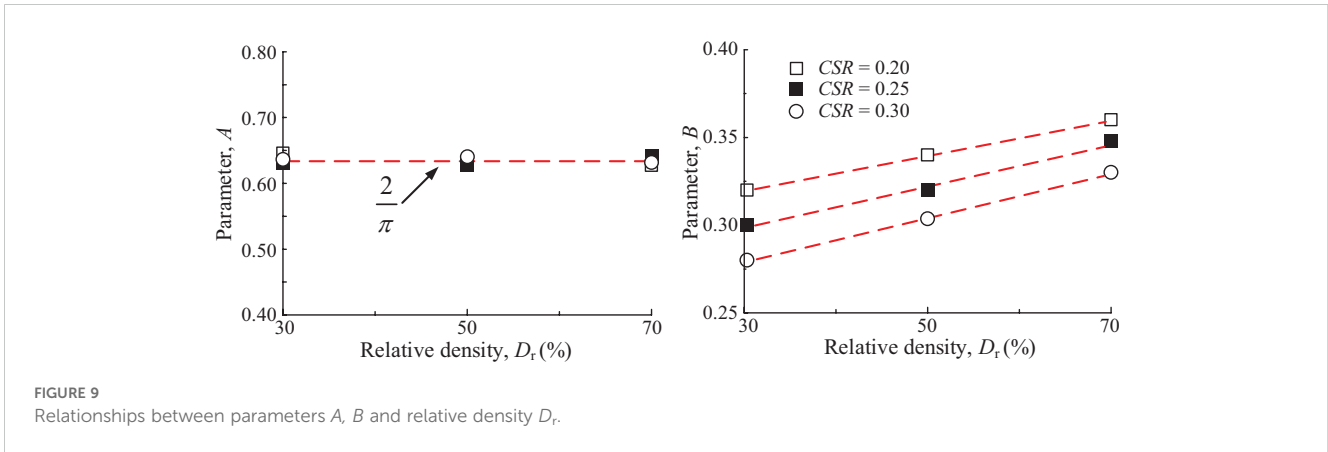
FIGURE 9
Relationships between parameters A, B and relative density D_r.
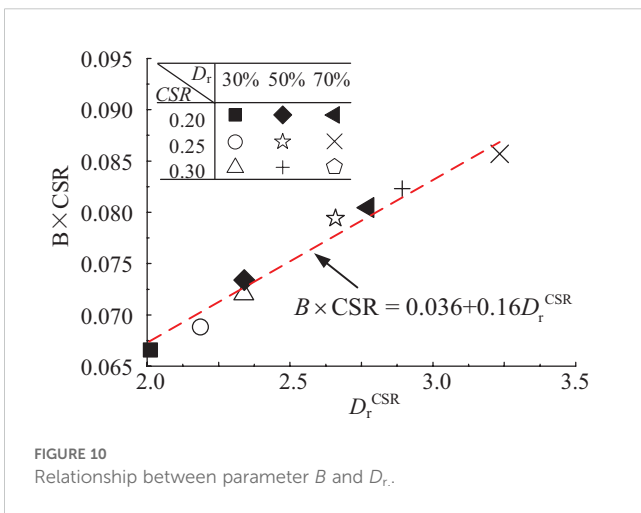

FIGURE 10
Relationship between parameter B and D_r.

$$E_r = \frac{2}{\pi} \arctan\left[\frac{0.036 + 0.16 D_r^{\text{CSR}}}{\text{CSR}} \times (N+1)\right] \quad (9)$$

4 Conclusions

In this study, we investigated the impacts of D_r, FC, and CSR on the dynamic elastic modulus $E_{d\text{-}N}$ of saturated coral sands with non-plastic fines and its development patterns, and drew the following conclusions:

(1) $E_{d\text{-}N}$ of saturated coral sands keeps accumulating with increasing N during cyclic loading, and it increases with increasing D_r and decreases with increasing FC during the loading process.

(2) The initial dynamic elastic modulus $E_{d\text{-}1}$ is affected by FC, D_r, and CSR. Alternatively, the steady-state dynamic elastic modulus $E_{d\text{-}s}$ is affected by the combined impact of FC and D_r and to a lesser extent by the CSR. Linear relationships between $E_{d\text{-}1}$ and e_{sk}^{*} and $E_{d\text{-}s}$ and e_{sk}^{*} for $FC < FC_{th}$ were established respectively by introducing the equivalent skeleton void ratio e_{sk}^{*}.

(3) The relative dynamic elastic modulus E_r is defined as the ratio of $E_{d\text{-}N}$ to $E_{d\text{-}s}$. E_r is not affected by the FC, but

TABLE 1 Test scheme.

ID	D_r(%)	FC (%)	CSR	ID	D_r(%)	FC (%)	CSR	ID	D_r(%)	FC (%)	CSR
1	30	0		13	30	0		25	30	0	
2	30	10		14	30	10		26	30	10	
3	30	20		15	30	20		27	30	20	
4	30	30		16	30	30		28	30	30	
5	50	0		17	50	0		29	50	0	
6	50	10		18	50	10		30	50	10	
7	50	20	0.20	19	50	20	0.25	31	50	20	0.30
8	50	30		20	50	30		32	50	30	
9	70	0		21	70	0		33	70	0	
10	70	10		22	70	10		34	70	10	
11	70	20		23	70	20		35	70	20	
12	70	30		24	70	30		36	70	30	

increases with increasing N. A prediction model for E_r in the form of an inverse tangent function was developed, and its fitting parameters A and B were analyzed.

Data availability statement

The original contributions presented in the study are included in the article/supplementary material. Further inquiries can be directed to the corresponding author.

Author contributions

RZ: Writing – original draft. ZH: Formal Analysis, Writing – review & editing. QL: Data curation, Investigation, Writing – original draft. QY: Project administration, Supervision, Validation, Writing – review & editing. QW: Writing – review & editing, Methodology.

Funding

Conflict of interest

Author HZ was employed by China Nuclear Power Engineering co.,Ltd. The remaining authors declare that the research was conducted in the absence of any commercial or financial relationships that could be construed as a potential conflict of interest.

Publisher's note

All claims expressed in this article are solely those of the authors and do not necessarily represent those of their affiliated organizations, or those of the publisher, the editors and the reviewers. Any product that may be evaluated in this article, or claim that may be made by its manufacturer, is not guaranteed or endorsed by the publisher.

References

ASTM International (2000). *D2487-00. Standard practice for classification of soils for engineering Purposes (Unified Soil Classification System)* (West Conshohocken, PA, USA: ASTM International).

ASTM International (2016a). *D4253-16. Standard test methods for maximum index density and unit weight of soils using a vibratory table* (West Conshohocken, PA, USA: ASTM International).

ASTM International (2016b). *D4254-16. Standard test methods for minimum index density and unit weight of soils and calculation of relative density* (West Conshohocken, PA, USA: ASTM International).

Catano, J., and Pando, M. A. (2012). "Static and dynamic properties of a calcareous sand from Southwest Puerto Rico," in *GeoFlorida 2010: Advances in Analysis*, Orlando, USA: Modeling & Design. 842–851. doi: 10.1061/41095(365)8

Chen, G. X., Liang, K., Zhao, K., and Yang, J. (2024). Shear modulus and damping ratio of saturated coral sand under generalised cyclic loadings. *Géotechnique* 74, 116–133. doi: 10.1680/jgeot.21.00181

Chen, G. X., Wu, Q., Zhao, K., Shen, Z. F., and Yang, J. (2020). A binary packing material-based procedure for evaluating soil liquefaction triggering during earthquakes. *J. Geotech. Geoenviron. Eng.* 146, 04020040. doi: 10.1061/(ASCE)GT.1943-5606.0002263

Deng, C. H., and Haigh, S. K. (2022). Sand deformation mechanisms mobilised with active retaining wall movement. *Géotechnique* 72, 260–273. doi: 10.1680/jgeot.20.P.041

Ding, Z., He, S. H., Sun, Y. F., Xia, T. D., and Zhang, Q. F. (2021). Comparative study on cyclic behavior of marine calcareous sand and terrigenous siliceous sand for transportation infrastructure applications. *Constr. Build Mater.* 283, 122740. doi: 10.1016/j.conbuildmat.2021.122740

Huang, C. X., Xu, S. K., Shen, Z. F., Zhang, L., Wang, L., and Liu, C. (2023). Effects of non-plastic fines on liquefaction properties of saturated silt using discrete element modeling. *Eng. Geo.* 317, 107091. doi: 10.1016/j.enggeo.2023.107091

Iwasaki, T., Tatsuoka, F., and Takagi, Y. (1978). Shear moduli of sands under cyclic torsional shear loading. *Soils Found.* 18, 39–56. doi: 10.3208/sandf1972.18.39

Jafarian, Y., and Javdanian, H. (2020). Dynamic properties of calcareous sand from the Persian Gulf in comparison with siliceous sands database. *Int. J. Civ. Eng.* 18, 245–249. doi: 10.1007/s40999-019-00402-9

Kallioglou, P., Tika, Th., and Pitilakis, K. (2008). Shear modulus and damping ratio of cohesive soils. *J. Earthq Eng.* 12, No. doi: 10.1080/13632460801888525//

Kantesaria, N., and Sachan, A. (2021). Cyclic degradation and pore-water pressure response of high-plasticity compacted clay. *J. Geotech Geoenviron. Eng.* 147, 04021113. doi: 10.1061/(ASCE)GT.1943-5606.0002630

Karatza, Z., Andò, E., Papanicolopulos, S.-A., Ooi, J. Y., and Viggiani, G. (2017). Evolution of deformation and breakage in sand studied using X-ray tomography. *Géotechnique* 68, 107–117. doi: 10.1680/jgeot.16.P.208

Liang, K., Chen, G. X., Du, X. L., Xu, C. S., and Yang, J. (2023). A unified formula for small-strain shear modulus of sandy soils based on extreme void ratios. *J. Geotech. Geoenviron. Eng.* 149, 04022127. doi: 10.1061/JGGEFK.GTENG-10913

Long, H., Zhuang, K., Deng, B., Jiao, J. L., Zuo, J. J., and You, E. L. (2022). Dynamic characteristics of coral sand in the condition of particle breakage. *Geofluids* 2022, 5304179. doi: 10.1155/2022/5304179

Ma, L. J., Deng, J. J., Wang, M. Y., Wang, J. P., Fang, B., and Wu, J. W. (2024b). Effect of diagenetic variation on the static and dynamic mechanical behavior of coral reef limestone. *Int. J. Min. Sci. Technol.* 34, 893–908. doi: 10.1016/j.ijmst.2024.07.004

Ma, L. J., Ke, L. W., Chen, T., Wu, J. N., Song, Y. J., and Xu, X. Y. (2024a). Dynamic mechanical behaviors of coral sand under drop weight impact. *Acta Geotech.* 19, 699–716. doi: 10.1007/s11440-023-01911-7

Mohammadi, A., and Qadimi, A. (2015). A simple critical state approach to predicting the cyclic and monotonic response of sands with different fines contents using the equivalent intergranular void ratio. *Acta Geotech.* 10, 587–606. doi: 10.1007/s11440-014-0318-z

Nong, Z. Z., and Park, S. S. (2021). Effect of loading frequency on volumetric strain accumulation and stiffness improvement in sand under drained cyclic direct simple shear tests. *J. Geotech. Geoenviron. Engng.* 147, 04021159. doi: 10.1061/(ASCE)GT.1943-5606.0002706

Rahman, M. M., Lo, S. R., and Gnanendran, C. T. (2008). On equivalent granular void ratio and steady state behaviour of loose sand with fines. *Can. Geotech. J.* 45, 1439–1455. doi: 10.1139/T08-064

Rollins, K. M., Evans, M. D., Diehl, N. B., and Daily, W. D. III (1998). Shear modulus and damping relationships for gravels. *J. Geotech. Geoenviron. Eng.* 124, 396–405. doi: 10.1061/(ASCE)1090-0241(1998)124:5(396

Rollins, K. M., Singh, M., and Roy, J. (2020). Simplified equations for shear-modulus degradation and damping of gravels. *J. Geotech. Geoenviron. Eng.* 146, 04020076. doi: 10.1061/(ASCE)GT.1943-5606.0002300

Seed, H. B., and Idriss, I. M. (1970). *Soil moduli and damping factors for dynamic response analyses, Report EERC 70-10* (Berkeley, CA, USA: University of California).

Thevanayagam, S. (2000). "Liquefaction potential and undrained fragility of silty sands," in *Proceedings of the 12th World Conference Earthquake Engineering CD-ROM* (New Zealand Society for Earthquake Engineering, Wellington, New Zealand).

Vucetic, M., and Mortezaie, A. (2015). Cyclic secant shear modulus versus pore water pressure in sands at small cyclic strains. *Soil Dynam. Earthq. Eng.* 70, 60–72. doi: 10.1016/j.soildyn.2014.12.001

Wen, B., Yuan, N. Z., Kong, L. W., and Chen, W. (2021). Application practice and settlement estimation of composite ground for high-rise building on coral sand site of hydraulic fill. *China Civil Eng. J.* 54, 85–93. doi: 10.15951/j.tmgcxb.2021.12.006

Wichtmann, T., Navarrete Hernández, M. A., and Triantafyllidis, T. (2015). On the influence of a non-cohesive fines content on small strain stiffness, modulus degradation and damping of quartz sand. *Soil Dyn. Earthq. Eng.* 69, 103–114. doi: 10.1016/j.soildyn.2014.10.017

Wu, Q., Liu, Q. F., Zhuang, H. Y., Xu, C. S., and Chen, G. X. (2022). Experimental investigation of dynamic shear modulus of saturated marine coral sand. *Ocean Eng.* 264, 112412. doi: 10.1016/j.oceaneng.2022.112412

Zhao, Z., Dong, Y., Zhang, Z. P., Gao, Y., and Zhang, X. S. (2022). Observed responses of a saturated sand under constant deviatoric stress path in drained triaxial tests over a range of applied shear stress. *Proc. Instit. Civil Eng. - Geotech. Eng.* 176, 453–460. doi: 10.1680/jgeen.21.00086